Journal of Power Sources 244 (2013) 403–409

Contents lists available at SciVerse ScienceDirect

Journal of Power Sources

journal homepage: www.elsevier.com/locate/jpowsour

Towards an all-solid-state battery: Preparation of conversion anodes by electrodeposition–oxidation processes

María C. López, Gregorio F. Ortiz, Pedro Lavela*, José L. Tirado

Laboratorio de Química Inorgánica, Universidad de Córdoba, Edificio Marie Curie, Campus de Rabanales, 14071 Córdoba, Spain

HIGHLIGHTS

- ► We propose a novel preparation route based on the electrodeposition of metals.
- ► The amorphous thin films have a large interfacial surface.
- ► The use of polymer binder and conductive carbon additives is avoided.
- ► Cell polarization and coulombic inefficiency are minimized.

ARTICLE INFO

Article history:
Received 20 September 2012
Received in revised form
28 November 2012
Accepted 1 December 2012
Available online 10 December 2012

Keywords:
Transition metal oxide
Thin film
Lithium battery
Mössbauer spectroscopy

ABSTRACT

A thin film electrode consisting of a mixture of iron and nickel oxides is prepared by a single route. Electrochemical deposition from Fe^{2+} and Ni^{2+} solutions on a titanium substrate and further thermal treatment at low temperature allowed obtaining a nanocomposite thin film of NiO and Fe_2O_3. The electrochemical studies performed on lithium cells assembled with this electrode material revealed the smallest irreversibility from first to second discharge ever reported during the conversion reactions of metal oxides at ~0.8 V. Unlike bulk transition metal oxides, the poorly-crystalline oxidized material exhibited an unusually low discharge polarization. The ^{57}Fe Mössbauer spectra of partially discharged and charged electrodes evidenced the reversibility of the conversion reaction with lithium and the efficiency of the recovery of the local environment of iron after the first cycle.

1. Introduction

All solid state batteries have gained a renewed attention as a way to overcome certain limitations in the present lithium-ion models. Thus, this concept provides undeniable advances for miniaturized electronic devices, improvements in shelf lives, prevention of electrolytes leakage and better performance with temperature [1]. On the other hand, the use of conversion reaction-based electrodes [2,3] for commercial Li-batteries is promising for future applications in systems that demand efficient energy storage, but there still needs to get rid of important drawbacks. Up to date, although transition metal oxides (TMO) exhibit at least from 2 to 8 times higher capacity vs. graphite, no Lithium-ion battery is commercialized under this concept because (i) the huge hysteresis, in terms of a loss in energy density, observed between cycles of discharge/charge has to be minimized and (ii) the irreversible capacity between the first and second cycle represents almost 50% of the total capacity (coulombic inefficiency). To overcome these problems, TMO have been prepared by different routes including sol–gel [4], reverse micelles [5], among others. Also, different morphologies and particle size have been evaluated to determine their effect in the electrochemical behavior in lithium cells [6,7].

The upcoming thin-film technologies are leading to real breakthroughs in the field of nanoscience with applications in energy storage [8,9], optics [10] or medicine [11]. We have previously shown that electrodeposition is an efficient and reliable technique for preparing 1-D Sn, Fe, SnO and Fe_2O_3 nanowires. Our syntheses of active materials were performed using a template-like method, by electrodeposition on layers of self-organized nanotubular titania ($ntTiO_2$), previously formed by a simple anodization process. We have shown that the resulting particle morphology can enhance the electrochemical performances not only for TiO_2 thin films but also SnO and Fe_2O_3 nanowires as negative electrodes in Li-ion Batteries (LIBs) [12,13]. However, the two main problems mentioned above were not solved at that time.

* Corresponding author. Tel./fax: +34 957 21 86 37.
E-mail address: iq1lacap@uco.es (P. Lavela).

0378-7753/$ – see front matter © 2012 Elsevier B.V. All rights reserved.
http://dx.doi.org/10.1016/j.jpowsour.2012.12.008

A completely new strategy for the preparation of transition metal oxides is proposed. This method combines electrodeposition followed by a mild thermal treatment to obtain the transition metal oxides. Coulombic efficiencies of ca. 85% were recently reported [14]. In this work, nanocomposite thin films containing NiO and Fe_2O_3 are prepared and the electrode materials are evaluated in lithium test cells. Moreover, the origin of this unusual and interesting behavior is studied by a combination of electrochemical and spectroscopic techniques which provide different clues for a better understanding of their attractive behavior.

2. Experimental

An electrolytic cell is assembled with a Pt wire and a Ti foil as auxiliary and working electrode, respectively. A glass reference electrode (Ag/AgCl) was used. The electrolytic solution is a 1:1 mixture of 0.02 M iron(II) sulfate and 0.02 M nickel(II) nitrate solutions. The electrodeposition experiments were carried out in air atmosphere at room temperature passing a current density of -5 mA cm^{-2} (referred to the working electrode area) through the cell during 20 min. A programmable galvanostat/potentiostat PGSTAT12 Autolab was used. The electrodeposition process was surveyed by recording potential–time curves. The electrodeposited films were then annealed at 450 °C for 2 h to obtain the transition metal oxides. The mass of active electrode material was estimated from a quantitative chemical analysis by ICP of the transition metal content in the thin film. For the sake of comparison, a reference sample was prepared by annealing a blend of nickel (Aldrich, nanosize activated powder with purity of 99.9+%) and iron (Merck, particle size 10 μm) fine powders under the same annealing conditions than the films.

X-ray diffraction was carried out in a Siemens D5000 instrument with Cu Kα radiation. The microstructure and surface morphology of the materials were characterized by using transmission and scanning electron microscopes (JEOL JEM 2100 and JEOL-SM6300 instruments). Swagelok™ type lithium test cells were assembled into an argon-filled glove box with moisture and oxygen levels less than 2 ppm. For this purpose, a lithium disk was used as counter electrode and a 1 M $LiPF_6$ (EC:DMC) solution as electrolyte. The working electrode consists of the as-prepared oxide thin film without any additives. The electrochemical tests were performed using an Arbin multichannel potentiostat/galvanostat systems. The galvanostatic discharge/charge experiences were performed at a rate of 25–50 μA cm^{-2}.

The chemical state and composition of the electrode materials were analyzed using X-ray Photoelectron Spectroscopy (XPS, SPECS Phobios 150MCD) using Mg Kα source and a chamber pressure of 4×10^{-9} mbar. ^{57}Fe Mössbauer spectra were recorded in transmission mode at room temperature on an EG&G constant accelerator spectrometer. All the isomer shifts are given relative to the center of the α-Fe. The experimental spectra were fitted to Lorentzian lines by using a least squares based method. The goodness of the fit was controlled by the usual χ^2 test.

3. Results and discussion

The voltammogram (at 10 mV s^{-1}) of the electrochemical deposition of the nanocomposite thin film of NiO and Fe_2O_3 on the Ti substrate was carried out from open circuit voltage to a cathodic potential limit of -2.5 V vs. Ag/AgCl (Fig. 1a). During the cathodic reaction, there was no reaction until ca. -1.0 V, in agreement with the oxidation state of the transition metals in the electrolyte solution. Then the deposition starts with an increase of the cathodic current below -1.0 V (vs. Ag/AgCl), which is attributed to the nucleation and growth of the transition metals.

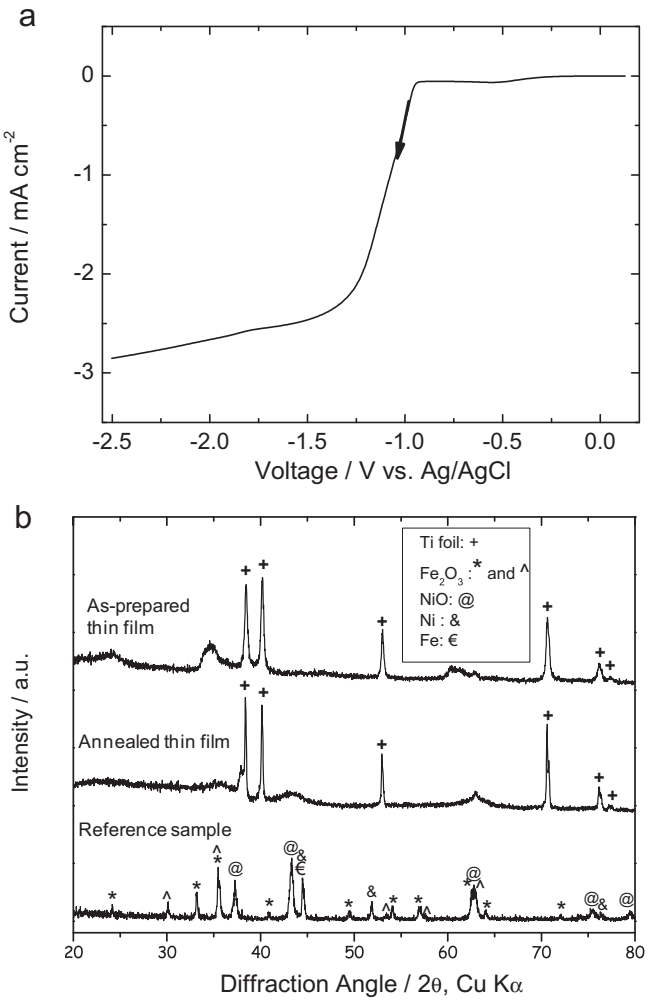

Fig. 1. (a) Voltammogram recorded at 10 mV s^{-1} of the Ni^{2+} and Fe^{2+} electrodeposition for the preparation of the thin film. (b) X-ray diffraction patterns of as-prepared, annealed thin film, and reference sample: Annealed mixture of crystalline Ni and Fe powders.

However, hydrogen evolution is also detected simultaneously to the Fe^{2+} and Ni^{2+} ion deposition at potentials more negative than -1.3 V. Consequently, a pH increase is expected in the vicinity of the electrode surface and the subsequent precipitation of metal hydroxides or hydrated oxides cannot be discarded [15]. Anyway, these as-prepared deposits showed poor electrochemical performance in lithium test cells. In this work, they are only considered as intermediates in the preparation of the annealed films which are characterized below in more detail.

The lack of well-defined reflections apart from the titanium substrate in the XRD pattern of the as-prepared and annealed FeNi deposits (Fig. 1b) allows neither proper phase identification nor calculating particle size. The oxidation state of iron and nickel in the deposits are determined below from XPS results. The XRD pattern of the reference sample, resulting from the annealing of a mixture of bulk nickel and iron, reveals a large number of reflections ascribable to Fe_2O_3 (JCPDS #33-0664; #39-1346) and NiO (JCPDS #44-1159) (Fig. 1b). In addition, several peaks were assigned to reflection of the initial metals such as Fe (JCPDS #06-0696) and Ni (JCPDS #04-0850). The presence of reflections ascribable to the elements evidences the difficulty to oxidize the large bulk particles in the same condition used for the thin film. On the other hand, the pattern corresponding to the oxidized thin film exhibits large

reflections ascribable to the titanium current collector. Also, broad and low intense peaks located around 35.5, 43 and 63° (2Θ) are detected corresponding to a mixture of Fe_2O_3 and NiO (Fig. 1b). Therefore, an inherent advantage of the electrochemical deposition technique is the suitable control of the amount and crystallinity of the electrodeposited species. We should highlight the X-ray amorphous character of oxidized binary FeNi thin films since, to the best of our knowledge, no previous studies have been reported yet.

Energy dispersive X-ray spectroscopy (EDX) analysis of the deposits obtained at a short time revealed the presence of Fe and Ni together with Ti from the current collector (Fig. 2a). Nitrogen adsorption isotherms (Fig. 2b) reveal a Type IV isotherm associated with capillary condensation taking place in mesopores. In fact, the pore size distribution curve shows a narrow signal at a value close to 2 nm. Considering Faraday's law, the estimated mass for electrodeposited FeNi-based materials is around 1.8 mg cm^{-2} for samples obtained at 20 min of deposition times. The transmission electron microscopy image in Fig. 3a shows particle morphology close to folded sheets with a thickness of only a few nanometers. A high magnification TEM image reveals the presence of nanocrystalline domains with diameters ranging between 5 and 10 nm (Fig. 3b). The Debye circles recorded in the selected area electron diffraction (SAED) pattern are ascribable to (012) and (110) reflections of NiO and (104) and (110) reflections of α-Fe_2O_3 (inset of Fig. 3b). Lattice fringes were only visible in a reduced number of regions in the sample, indicating that this material is nanocrystalline rather than amorphous. Cross-sectional views of the film from SEM images (Fig. 3c), revealed a thickness of ca. 5 μm.

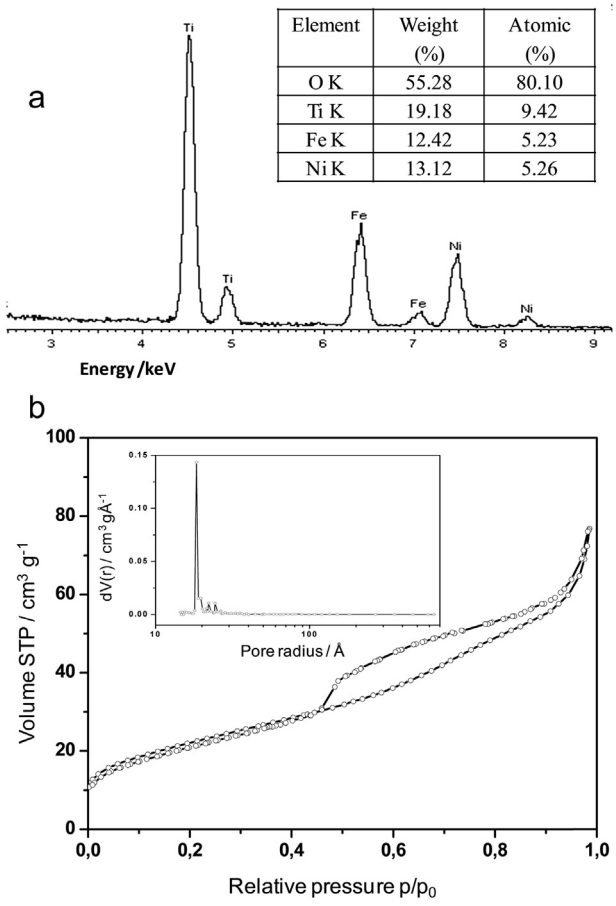

Element	Weight (%)	Atomic (%)
O K	55.28	80.10
Ti K	19.18	9.42
Fe K	12.42	5.23
Ni K	13.12	5.26

Fig. 2. (a) Energy dispersive X-ray spectroscopy (EDX) analysis of the thin film. (b) Nitrogen adsorption and desorption isotherm (inset: pore size distribution) of the thin film.

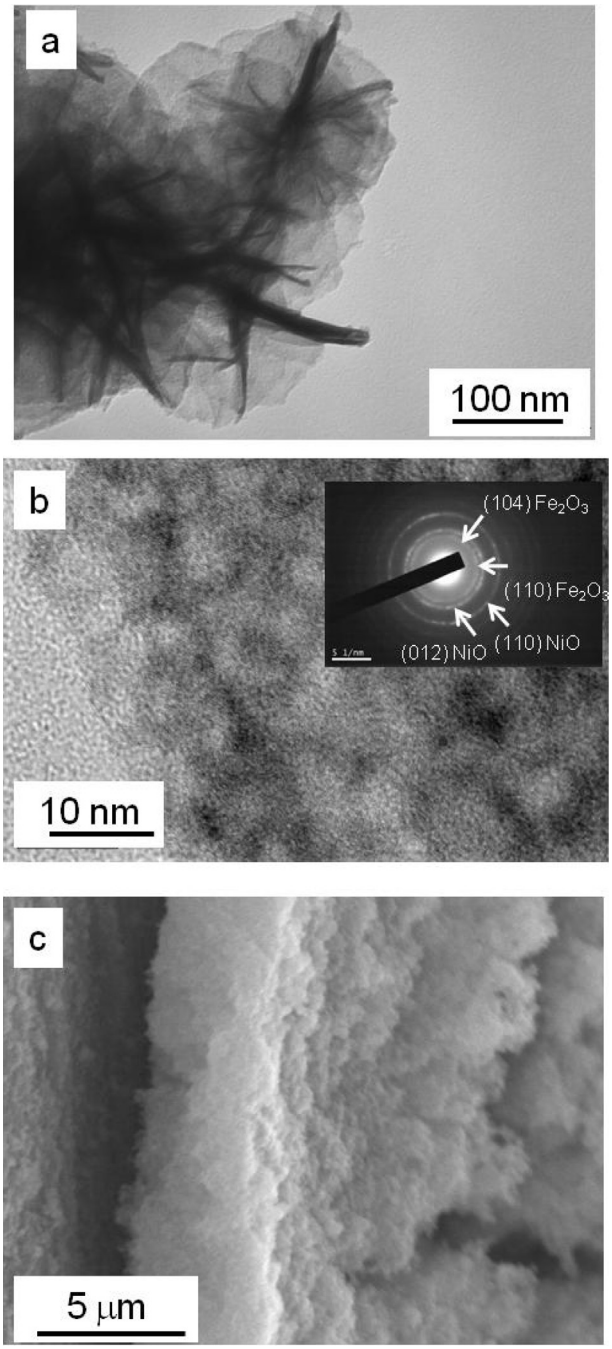

Fig. 3. Electron microscope images of the thin film. a) Low magnification TEM image; b) High magnification image showing the nanocrystalline particles. (Inset: SAED pattern on the showed particle); c) SEM image of thin film edge.

The XPS spectra of as-prepared samples before thermal annealing show Fe^{3+} and Ni^{2+} ions exclusively (Fig. 4). The as-prepared deposits showed poor electrochemical response and were discarded for further study, In contrast, the electrochemical performance of annealed deposits was significantly better, as shown below, probably due to their quantitative conversion to oxides, as shown by the SAED results (Fig. 3). The surface of the annealed thin film was analyzed by XPS (Fig. 5). The sample was subjected to Ar^+ ion etching at different times (1, 6, 16, 36 and 86 min) to deeply identify the composition of the entire film. The XPS spectrum measured on the outer surface of the annealed thin film shows that the Fe 2p core levels are split into $2p_{1/2}$ and $2p_{3/2}$

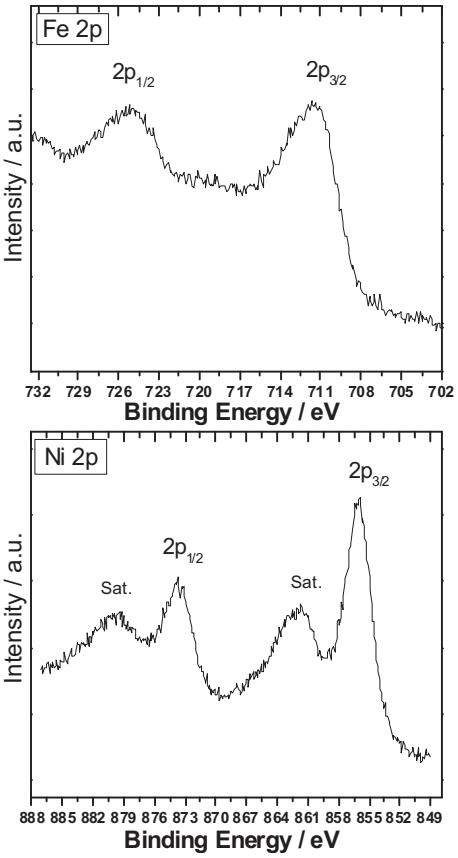

Fig. 4. XPS spectra of the as-prepared thin film before thermal annealing for the Fe 2p and Ni 2p levels.

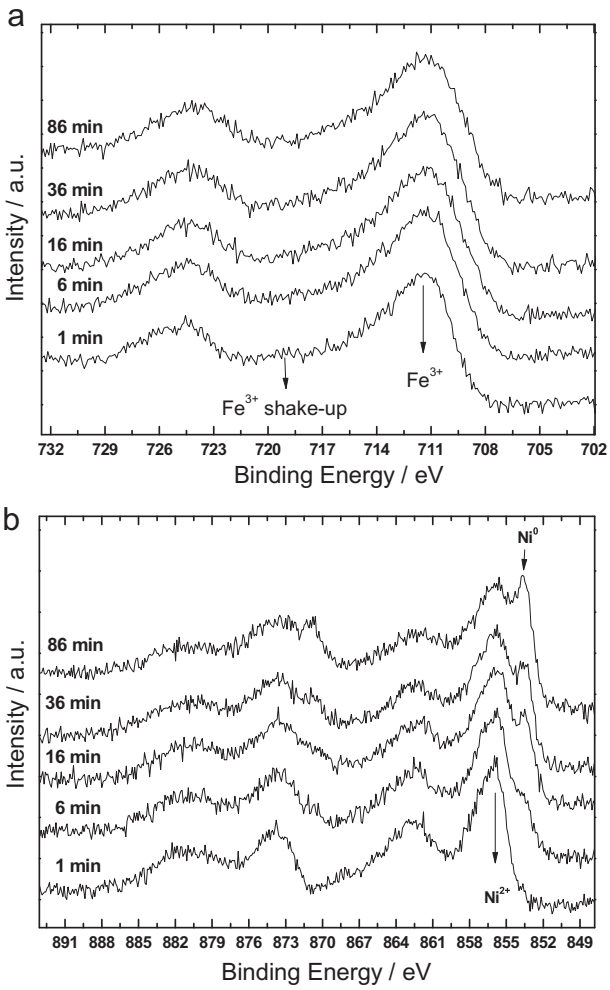

Fig. 5. XPS spectra of the thin film after thermal annealing recorded after several periods of time of Ar^+ ion etching for the (a) Fe 2p and (b) Ni 2p levels.

components, due to the spin-orbit coupling (Fig. 5a). The signal detected at 711.4 eV is ascribable to Fe^{3+}. The shake-up satellite line characteristic of Fe^{3+} species is visible at 719 eV. This feature is common in Fe_2O_3-containing materials [16–18]. The Ni 2p spectra are shown in Fig. 5b. The Ni $2p_{3/2}$ peak at 856 eV and Ni $2p_{1/2}$ peak at 873.4 eV reveal the presence of Ni^{2+} ions [19,20]. The depth profile analysis revealed some interesting features after a long Ar-etching treatment. The small Fe $2p_{3/2}$ satellite peak at 719 eV progressively disappears and a lower binding energy Ni $2p_{3/2}$ peak is observed. The reduction of nickel oxides in the argon ion beam is an effect previously described in the literature [18]. This is the most plausible interpretation to the presence of metallic nickel lines in the spectra of Fig. 5b.

The lithium driven conversion reaction is a well known mechanism allowing a high density and reversible lithium storage in transition metal compounds [3–6]. Transition metals are completely reduced to their metallic state, hence, promoting a large electron transfer per formula unit. Their low working voltages involve their use as potential anodes in Li-ion batteries. Fig. 6a shows the voltage versus capacity curve performed on a reference sample consisting of the mixture of bulk NiO and Fe_2O_3. As can be seen, the length of the first discharge plateaus reflects fairly well the extent of Fe^{3+} and Ni^{2+} reduction. A significant irreversible effect can be observed at the end of the charge. The second discharge plateau is shifted to 1.3 V (Fig. 6b) in comparison with the main reduction plateaus at 1.05 and 0.7 V observed in the first discharge.

Changes in the potential of the conversion reaction may have a significant impact on the surface area and surface energy changes as previously reported [21]. If such effects are taken into account we should observe a change in the potential (V) in the oxidized NiFe (Fig. 7) and thus admit that during electrochemical reactions with Li a remarkable increase in surface area take place. Indeed, such postulation is confirmed for some oxidized singular and binary metal reported in the literature by the observation of such potential deviation from the first to the second discharge [21,22] and is also visible in our results plotted in Fig. 7. Several reports have demonstrated the benefits of using nanocrystalline TMO as electrode materials for conversion reactions [6,7]. However, the shift in cell potential and the irreversible capacity after the first cycle has not been largely diminished.

The voltage versus capacity plot recorded for the electrodeposited sample shows a different profile (Fig. 7a and b). The abrupt decrease of voltage observed in the highly crystalline sample is replaced by a sloping voltage accounting for 400 μA h cm^{-2}. Then, a short quasi-plateau is spread over 350 μA h cm^{-2}. These electrochemical features are clearly identified in the derivative curve by an anodic broad band at 1.4 V and an anodic narrow peak at 0.8 V, respectively. At the end of the discharge, cell potential smoothly decreases to the lower cut-off voltage, which is ascribable to a reversible pseudo-capacitive behavior. During the first charge, the profile of the derivative curve showed two broad and low intense bands placed at ca. 1.3 V and 2.3 V, ascribable to the metal oxidation. From the inspection of Figs. 6 and 7, we can observe that the irreversibility after the first charge is significantly reduced as

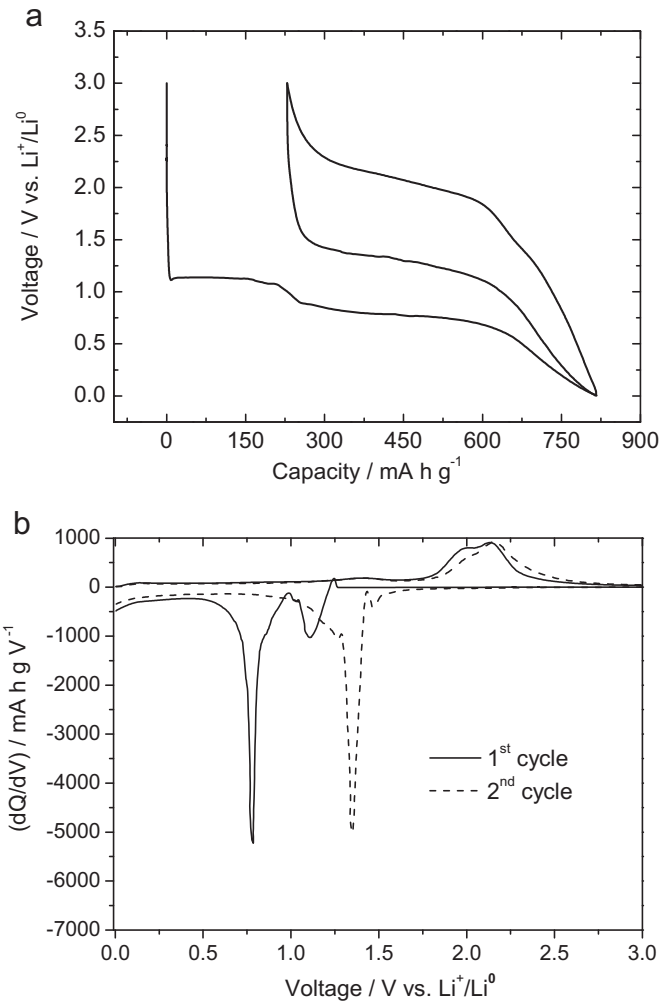

Fig. 6. Galvanostatic curves for the reference sample (a) Voltage versus capacity and (b) derivative curve.

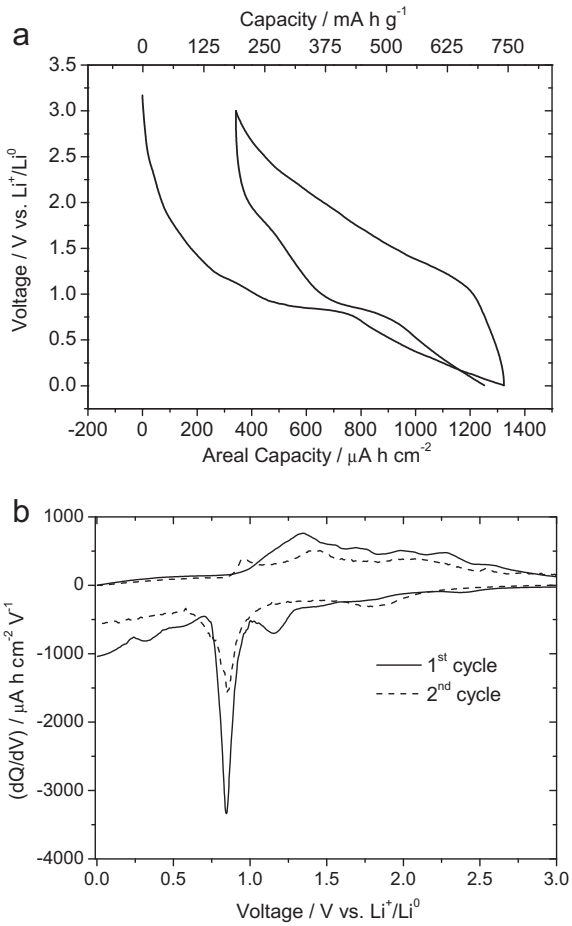

Fig. 7. Galvanostatic curves for thin film (a) Voltage versus capacity (areal and gravimetric scales) and (b) derivative curve.

compared to the bulk TMO. Another interesting feature is the low voltage shifting between the first and second discharge that revealed an improved reversibility of the nanocrystalline thin film. Thus, it is clearly evident that our novel amorphous TMO thin film sample exhibits a distinctive electrochemical behavior upon cycling in terms of discharge polarization and irreversibility in first cycle. As a matter of fact, the minimal polarization of electrodes is consistent solely with the presence of X-ray amorphous TMO films, which are similar to those found when starting with bulk oxides after cycling the cells. The cell capacity values were recorded for a number of cycles for both the thin film and bulk oxides (Fig. 8). It is quite evident the poor performance of the bulk material which initial capacity value of 816 mAh g^{-1} decreases quickly to 235 mAh g^{-1} after only 10 cycles. Otherwise, the thin film samples kept a capacity value of 353 mAh g^{-1} after the same number of cycles. This result confirms the validity of this electrode design to optimize the electrochemical behavior of transition metal oxides in lithium driven conversion reactions.

^{57}Fe Mössbauer spectroscopy is a helpful technique to unfold the changes of oxidation state and local environments of the probe atom. The spectrum of the original sample shows a largely-broadened split signal that can be decomposed in two super-paramagnetic doublets ascribable to two different local environments for Fe(III) ions (Fig. 9 and Table 1). It differs from the spectra recorded for bulk material in which the ferromagnetic effect is visible. In the latter case, one or more sextets appear for the Fe^{3+} ions. For nanometric particles, the magnetic interaction between magnetic domains disappears and the solid becomes super-paramagnetic [23,24]. Due to the lack of crystallinity in this sample, their assignment to crystallographic sites is precluded. The signal with the large value is ascribable to a high anisotropy in the charge distribution and hence to iron atoms located at the particle surface. The significant contribution of this signal is related to the low

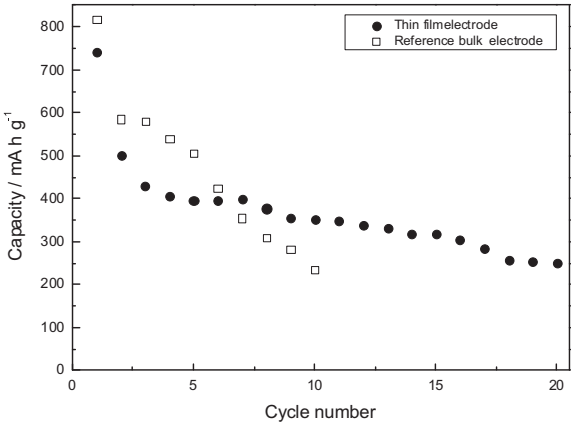

Fig. 8. Plot of capacity versus cycle number of the studied electrodes.

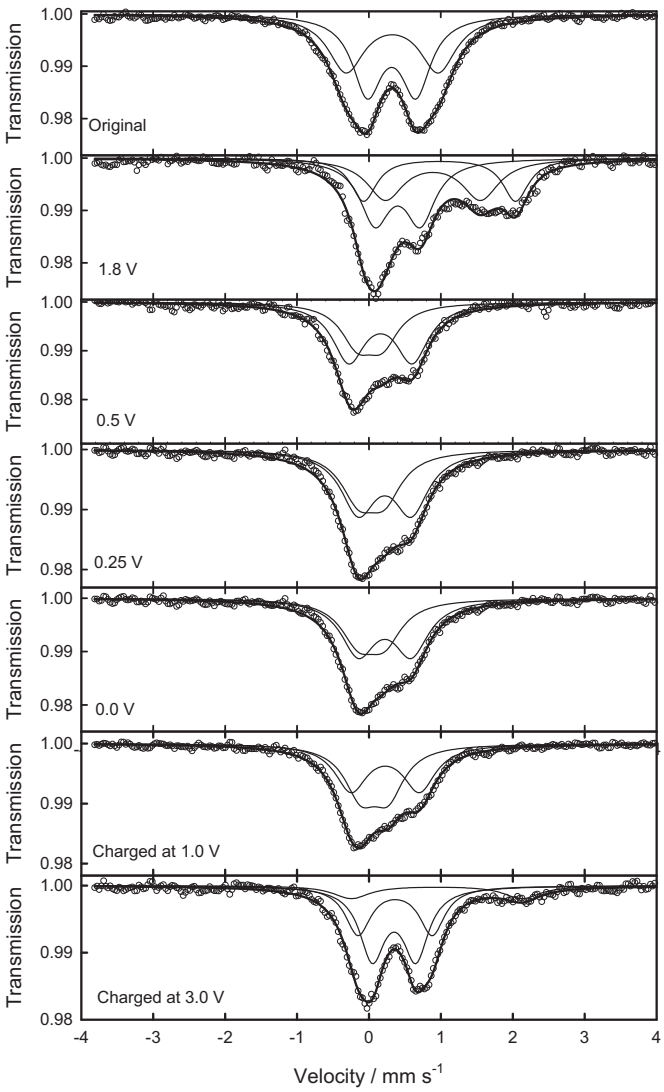

Fig. 9. ^{57}Mössbauer spectra of the original sample and partially discharged and charged electrodes.

Table 1
Hyperfine parameters of the deconvoluted Mössbauer spectra of the original sample and partially discharged and charged electrodes.

Sample	δ (mm s^{-1})	Δ (mm s^{-1})	Γ (mm s^{-1})	C (%)	χ^2
Original	0.32(1)	0.68(2)	0.50(2)	52.4	0.672
	0.32(2)	1.28(3)	0.61(2)	47.6	
1. 8 V	0.40(1)	0.63(2)	0.51(2)	41.6	0.875
	0.89(2)	1.32(3)	0.62(3)	33.4	
	0.98(1)	2.11(2)	0.43(3)	24.9	
0.5 V	0.16(1)	0.88(2)	0.55(5)	60.5	0.567
	0.01(1)	0.35(2)	0.55(2)	39.5	
0.25 V	0.20(2)	0.79(4)	0.59(3)	56.7	0.562
	−0.02(3)	0.39(5)	0.58(5)	43.3	
0.0 V	0.219(2)	0.73(4)	0.58(4)	57.7	0.634
	0.03(3)	0.36(6)	0.59(5)	42.3	
Charged at 1 V	0.226(8)	0.95(1)	0.54(5)	49.5	0.509
	0.076(7)	0.38(1)	0.55(4)	50.5	
Charged at 3 V	0.35(1)	0.61(1)	0.42(1)	51.2	0.571
	0.36(1)	1.03(2)	0.42(3)	35.1	
	0.94(4)	2.37(6)	0.62(9)	13.7	

δ: isomer shift; Δ: quadrupole splitting; Γ: line-width at half maximum; C: contribution/concentration; χ^2: goodness of the fitting.

particle size of the nanocrystalline material. Conversely, the low split signal could be assigned to iron atoms inside the particle.

Spectra of partially discharged and charged electrodes were recorded at room temperature (Fig. 9). The deconvolution of the spectrum recorded on a sample discharged at 1.8 V revealed the appearance of two new and highly split signals centered at 0.89 and 0.98 mm s^{-1} (Table 1). These signals are ascribed to Fe^{2+} ions as intermediate in the reduction of the ferric ions to their metallic state. Another sample was discharged at 0.5 V corresponding to the end of the plateau at 0.8 V. At this point, the spectrum profile evidences the disappearance of the signals assigned to Fe^{2+}. Their deconvolution resulted in two doublets with distinct quadrupole. Similarly to the approach applied to the original sample, the different quadrupole splitting values can be related to the location of iron atoms at either the surface or the core of the particle. The efficiency of the electrochemical reduction is evidenced by the decrease of the isomer shift values mainly observed for the low split signal. Contrarily, the isomer shift values for the high split signal range from 0.16 to 0.22 mm s^{-1}. It can be explained in terms of parallel oxidation reactions of surface iron atoms in close contact to the electrolyte [25,26]. On charging, an increase of the isomer shift values to 0.35 and 0.36 mm s^{-1} is indicative of the electrochemical oxidation of the iron atoms to the trivalent state. The quadrupole splitting values of the sample charged at 3 V are also similar to those of the original sample. This fact is related to a good reversibility and an efficient recovery of the trivalent oxidation state for iron. Only a minor decrease of the relative contribution of the highly split doublet could be indicative of a slight decrease in the population of iron atoms at the particles surface and consequently an increase of particle size. Also, a weak contribution of Fe^{2+} remains visible after charging. Kinetic effects can be responsible for the presence of a small population of Fe^{2+} ions at the core of the particles whose oxidation was not completed at the end of the charge.

4. Conclusions

In the light of the above results, the use of nanocomposite thin films with large amount of interfacial surface and no binder or conducting additives as conversion electrodes can minimize first cycle irreversibility and cell polarization during cycling. We propose a novel preparation procedure based on the electrochemical deposition from Fe^{2+} and Ni^{2+} solutions on a titanium substrate followed by mild thermal treatment, which leads to a nanocomposite thin film of NiO and Fe_2O_3. The resulting nanocrystalline thin film exhibited a good electrochemical behavior in terms of coulombic efficiency observed in the first cycle and minimal discharge polarization. Such enhancement is most probably due to the combined nanocrystalline and thin film character of the starting material. Maximum first-discharge capacities of around 740 mA h g^{-1} are achieved in the first cycle. These results reveal new pathways to minimize cell polarization and coulombic inefficiency in electrode material undergoing lithium driven conversion reaction with potential application in Li-ion batteries.

Acknowledgments

The authors are grateful to Junta de Andalucía for financial support (Contract FQM-6017 and FQM-7206), MICINN (MAT2011-22753). We thank to UCO-SCAI, IUIQFN and ERI_ALISTORE. Gregorio F. Ortiz is indebted to the 'Ramón y Cajal' program (RYC-2010- 05596). We also acknowledge the National Center of Electronic Microscopy from "Universidad Complutense de Madrid", for helpful assistance in the TEM study.

References

[1] P.H.L. Notten, F. Roozeboom, R.A.H. Niessen, L. Baggetto, Adv. Mater. 19 (2007) 4564.
[2] M.M. Thackeray, S.D. Baker, K.T. Adendorff, J.B. Goodenough, Solid State Ionics 17 (1985) 175.
[3] P. Poizot, S. Laruelle, S. Grugeon, L. Dupont, J.M. Tarascon, Nature 407 (2000) 496.
[4] P. Lavela, J.L. Tirado, J. Power Sources 172 (2007) 379.
[5] C. Vidal-Abarca, P. Lavela, J.L. Tirado, J. Power Sources 196 (2011) 6978.
[6] P. Lavela, J.L. Tirado, C. Vidal-Abarca, Electrochim. Acta 52 (2007) 7986.
[7] J.Y. Xiang, J.P. Tu, L. Zhang, Y. Zhou, X.L. Wang, S.J. Shi, J. Power Sources 195 (2010) 313.
[8] G.F. Ortiz, I. Hanzu, T. Djenizian, P. Lavela, J.L. Tirado, P. Knauth, Chem. Mater. 21 (2009) 63.
[9] M.M. Shaijumon, E. Perre, B. Daffos, P.L. Taberna, J.M. Tarascon, P. Simon, Adv. Mater. 22 (2010) 4978.
[10] C. Jung, P. Schwaderer, M. Dethlefsen, R. Kohn, J. Michaelis, C. Brauchle, Nat. Nanotechnol. 6 (2011) 86.
[11] X. Cheng, E. Yegan Erdem, S. Takeuchi, H. Fujita, B.D. Ratner, K.F. Bohringer, Lab Chip 10 (2010) 1079.
[12] G.F. Ortiz, I. Hanzu, P. Lavela, P. Knauth, J.L. Tirado, T. Djenizian, Chem. Mater. 22 (2010) 1926.
[13] G.F. Ortiz, I. Hanzu, P. Lavela, J.L. Tirado, P. Knauth, T. Djenizian, J. Mater. Chem. 20 (2010) 4041.
[14] G.F. Ortiz, J.L. Tirado, Electrochem. Commun. 13 (2011) 1427.
[15] U. Lacnjevac, B.M. Jovic, V.D. Jovic, Electrochim. Acta 55 (2009) 535.
[16] K. Wandelt, Surf. Sci. Rep. 2 (1982) 1.
[17] W. Weiss, W. Ranke, Prog. Surf. Sci. 70 (2002) 1.
[18] A.G. Fitzgerald, G. Muir, Surf. Interface Anal. 8 (1986) 247.
[19] J.A. Schreifels, P.C. Maybury, W.E. Swartz, J. Catal. 65 (1980) 195.
[20] Y.E. Roginskaya, O. Morozova, E. Lubnin, Y.Y. Ulitina, G. Lopukhova, S. Trasatti, Langmuir 13 (1997) 4621.
[21] J. Cabana, L. Monconduit, D. Larcher, M.R. Palacin, Adv. Mater. 22 (2010) E170.
[22] E. Hosono, S. Fujihara, I. Honma, H. Zhou, Electrochem. Commun. 8 (2006) 284.
[23] R. Alcántara, M. Jaraba, P. Lavela, J.L. Tirado, J.C. Jumas, J. Olivier-Fourcade, Electrochem. Commun. 5 (2003) 16.
[24] D. Larcher, D. Bonnin, R. Cortes, I. Rivals, L. Personnaz, J.M. Tarascon, J. Electrochem. Soc. 150 (2003) A1643.
[25] C. Vidal-Abarca, P. Lavela, J.L. Tirado, Solid State Ionics 181 (2010) 616.
[26] P. Lavela, J.L. Tirado, M. Womes, J.C. Jumas, J. Phys. Chem. C 113 (2009) 20081.